Raman amplification of optical pulses in silicon nanowaveguides: Impact of spectral broadening of pump pulses

Alexandre Baron
alexandre.baron@institutoptique.fr
Laboratoire Charles Fabry de l'Institut d'Optique, CNRS, Univ Paris-Sud, Campus Polytechnique, RD128, 91127 Palaiseau Cedex, France

Nicolas Dubreuil
Laboratoire Charles Fabry de l'Institut d'Optique, CNRS, Univ Paris-Sud, France

Philippe Delaye
Laboratoire Charles Fabry de l'Institut d'Optique, CNRS, Univ Paris-Sud, France

Robert Frey
Laboratoire Charles Fabry de l'Institut d'Optique, CNRS, Univ Paris-Sud, France

Govind P. Agrawal
Institute of Optics, University of Rochester, Rochester, New York, 14627, USA

We consider the Raman amplification problem for silicon waveguides in the regime in which both the pump and signal pulses are relatively short but wide enough that their duration exceeds the phonon lifetime (about 3 ps in silicon). We use the coupled pump-signal equations for numerical simulations that include all competing nonlinear effects such as self- and cross-phase modulations, two-photon and free-carrier absorptions, and changes in the refractive index induced by the free carriers. However, numerical simulations do not provide much physical insight. For this reason, we also develop an approximate analytic approach for solving the Raman amplification problem. We introduce the concept of an effective Raman gain and show analytically how it depends on the pump bandwidth. As the pump spectrum broadens inside the silicon waveguide, the effective Raman gain is reduced considerably. We obtain an analytical form of the nonlinear phase accumulated during propagation inside a silicon waveguide and use it to calculate the total spectral broadening experienced by a pump pulse. Using this result, we can predict changes in the effective Raman gain as a function of pump pulse energy. A comparison of our predictions with the recent experimental data shows that our model is reasonable and captures the essential physics. [DOI: 10.2971/jeos.2011.11030]

Keywords: nonlinear optics, nonlinear slow-mode waveguides, stimulated Raman scattering, self-phase modulation, Silicon Raman amplifier

1 INTRODUCTION

Silicon-on-insulator (SOI) technology has attracted a great deal of attention in recent years owing to its potential for on-chip optical data processing [1, 2]. The field of silicon photonics is motivated mostly by the need for optical interconnects [3, 4], amplifiers [5]–[8] and switches [9, 10]. Silicon is a promising platform because it exhibits relatively large values of the important nonlinear parameters such as the Kerr coefficient (n_2) and the Raman gain coefficient. Furthermore, the availability of high-quality SOI wafers from the microelectronics industry, coupled with a mature fabrication process, makes it possible to build ultracompact devices with tight confinement of optical modes [5, 11]. These localized modes enable nonlinear interaction at relatively low-power levels inside short nanowaveguides (typically 1 cm long). This is why much effort has been put into investigating nonlinear effects such as self- and cross-phase modulations (SPM and XPM) [5], [12]–[14], two-photon and cross two-photon absorptions (TPA and XPA), free-carrier absorption and refraction (FCA and FCR) [15, 16], stimulated Raman scattering (SRS) [5, 6, 15, 17], and four-wave mixing [18, 19]. SRS in particular has been extensively studied for providing optical amplification when a silicon nanowire is pumped with a continuous-wave (CW) or pulsed beam [5, 7, 8, 20, 21]. By 2005, Raman lasers operating in the CW [22] and pulsed regimes had been demonstrated [23].

In any theoretical model developed for understanding Raman amplification of short optical pulses under pulsed pumping, it is crucial to consider the interplay among all third-order nonlinearities to understand how they may impact the SRS process. For example, TPA, XPA, and FCA reduce the intensity of both pump and probe waves, leading to a reduced effective gain of the Raman amplifier [2, 11]. Since the phonon lifetime is close to 3 ps in crystalline silicon, one should be able to amplify picosecond pulses efficiently if their repetition rate is relatively low because the impact of FCA is strongly reduced for pulses shorter than 10 ps [7, 21, 24, 25]. Indeed, Solli *et al.* [26] have proposed the use of SPM- and FCR-induced spectral broadening of pump pulses to create broadband Raman amplifiers. In contrast, Kroeger *et al.* [5] have recently shown experimentally that this broadening can be detrimental to SRS because it causes saturation of the Raman gain. Their results show that, when the spectral bandwidth of the pump pulse becomes larger than the Raman-gain bandwidth (about 105 GHz), the Raman-gain coefficient is reduced considerably.

In this paper, we provide a theoretical basis for this experi-

Received January 21, 2011; published June 02, 2011

mental observation based on the coupled pump-signal equations developed for silicon waveguides [11]. Numerical simulations performed with the split-step Fourier method [27] using parameters for the device used in the experiment [5] show the reduction of the Raman gain observed experimentally. To provide further insight, we also solve the coupled pump-signal equations analytically with appropriate simplifying assumptions. In particular, we investigate how the TPA, SPM and FCR processes influence the reduction in the Raman gain by studying analytically the spectral broadening of pump pulses that they produce. The paper is organized as follows. In Section 2, we consider all nonlinearities that may occur in a silicon waveguide and present the coupled pump-signal equations used to solve the Raman amplification problem. Section 3 focuses on solving the coupled pump-signal equations approximately in the specific case in which the spectra of both pump and signal pulses as well as the Raman gain spectrum can be approximated with Gaussian functions. In Section 4, we include the remaining nonlinear phase effects (SPM, XPM, and FCR) and use the second-order moment to obtain an expression for the effective Raman gain coefficient in the presence of spectral broadening of pump pulses. We compare our predictions with the experimental measurements in Section 5 and draw some general conclusions.

2 The complete numerical model

We consider the experimental situation in which the pump and signal pulses with carrier frequencies ω_p and ω_s, respectively, are launched into a silicon waveguide. These pulses interact through SRS that transfers energy from the pump to the signal pulse. At the same time, both pulses are affected by linear losses, nonlinear losses (TPA and XPA), and nonlinear phase shifts (SPM, and XPM). Moreover, free carriers generated through TPA and XPA also affect the two pulses through FCA and FCR. All of these processes have been included in Ref. [11] to derive a set of two coupled pump-signal equations that form our starting point.

2.1 Coupled pump–signal equations

We use Maxwell's equations with the total electric field in the form

$$\begin{aligned}\mathbf{E}(x,y,z,t) = \hat{e}\mathrm{Re}\{&F_s(x,y)A_s(z,t)\exp[i(k_s z-\omega_s t)]\\ &+F_p(x,y)A_p(z,t)\exp[i(k_p z-\omega_p t)]\},\end{aligned} \tag{1}$$

where A_s and A_p are the slowly varying envelopes of the signal and pump fields (of intensity $|A_s|^2$ and $|A_p|^2$ respectively) with mode profiles F_s and F_p, respectively, and $\hat{e}$ is the polarization unit vector. The use of this form with the appropriate forms of the induced polarization inside the silicon waveguide leads to the following set of two coupled equations [11]:

$$\begin{aligned}\frac{\partial A_s}{\partial z} = &R(z,t)A_p(z,t)-\left(\frac{\alpha_l}{2}+f_s^2\sigma_c N_{fc}(z,t)\right)A_s(z,t)\\ &+ik_s f_s^2[2f_p^2 n_2(1+ir_s)|A_p(z,t)|^2\\ &+k_c N_{fc}(z,t)]A_s(z,t),\end{aligned} \tag{2}$$

$$\begin{aligned}\frac{\partial A_p}{\partial z} = &-R^*(z,t)A_s(z,t)-\left(\frac{\alpha_l}{2}+f_p^2\sigma_c N_{fc}(z,t)\right)\\ &\times A_p(z,t)+ik_p f_p^2[f_p^2 n_2(1+ir_p)|A_p(z,t)|^2\\ &+k_c N_{fc}(z,t)]A_p(z,t),\end{aligned} \tag{3}$$

where Raman amplification is included through

$$\begin{aligned}R(z,t) = if_p^2 f_s^2 g_R\frac{\Gamma_R}{\Omega_R}\int_{-\infty}^{t}\Big(&h_R(t-t')\exp[-i\Omega_{ps}(t-t')]\\ &\times A_s(z,t')A_p^*(z,t')\Big)\,dt'\end{aligned} \tag{4}$$

with $\Omega_{ps} = \omega_p - \omega_s$. Here g_R is the Raman gain coefficient (units m/W) and $h_R(t)$ is the Raman response function whose Fourier transform is given by [11]

$$\widetilde{H}_R(\Omega) = \frac{\Omega_R^2}{\Omega_R^2-\Omega^2-2i\Gamma_R\Omega}. \tag{5}$$

The parameters Ω_R and Γ_R characterize the Raman gain spectrum and represent the Raman shift ($\Omega_R/2\pi \approx 15.6$ THz) and the gain bandwidth ($\Gamma_R/\pi \approx 105$ GHz) related inversely to the phonon lifetime of about 3 ps in silicon at room temperature.

Equations (2)–(4) are identical to those appearing in Ref. [11] except that we have neglected the dispersion term because its contribution is relatively small ($\beta_2 \approx -1$ ps^2/m) for the silicon ridge waveguide that we wish to study [5]. We have also explicitly added the local-field factors f_p and f_s defined as $f_m^2 = n_{gm}/\bar{n}_m$ $(m = p,s)$ [5], [28]–[31], where $\bar{n}_m$ and n_{gm} represent the effective mode index and group index at the pump or signal frequencies. k_m $(m = p,s)$ is the pump or signal wave vector in air. Other parameters appearing in these equations represent various physical phenomena: α_l accounts for linear waveguide losses, n_2 is the Kerr parameter, $r_m = \beta_{\mathrm{TPA}}/(2k_m n_2)$ $(m = p,s)$ is a dimensionless parameter indicating the relative importance of the TPA parameter β_{TPA} compared to the Kerr effect, σ_c accounts for FCA, and k_c represents the free-carrier induced index changes (FCR). The presence of a factor 2 in front of $f_p^2 n_2(1+ir_s)$ in Eq. (2) is because of the cross-Kerr and cross-TPA (XPA) effects. Here, we neglect the dispersion of the Kerr and TPA coefficient between pump and signal, such that $\beta_{\mathrm{XPA}} = 2\beta_{\mathrm{TPA}}$ and $n_{2X} = 2n_2$, where n_{2X} is the cross-Kerr coefficient.

Later, we consider the simplest model of Raman amplification in which all nonlinear effects except SRS are ignored. In this case, the coupled pump–signal equations reduce to the following two coupled equations:

$$\frac{\partial A_s}{\partial z} = R(z,t)A_p(z,t)-\frac{\alpha_l}{2}A_s(z,t), \tag{6}$$

$$\frac{\partial A_p}{\partial z} = -R^*(z,t)A_s(z,t)-\frac{\alpha_l}{2}A_p(z,t). \tag{7}$$

2.2 Rate equation for the density of free carriers

The coupled pump–signal equations (2) and (3) contain the density N_{fc} of free carriers that are generated through TPA,

and we cannot solve them without adding a rate equation for N_{fc}. The primary TPA process is the one in which both photons come from the pump pulse (governed by β_{TPA}). In general, however, one should also include cross absorption (XPA), a process where one signal photon is absorbed together with a pump photon. If dispersion of the TPA coefficient is small between the pump and signal wavelengths, $\beta_{\mathrm{XPA}} = 2\beta_{\mathrm{TPA}}$. We neglect the influence of the XPA process in generating free-carriers by assuming that the signal intensity $|A_s(z,t)|^2$ is much weaker than the pump intensity $|A_p(z,t)|^2$ at all distances within the silicon waveguide. However, its influence on the absorption of the signal intensity is not negligeable and must be conserved in Eq. (2). With this assumption, the free-carrier density N_{fc} satisfies the following rate equation:

$$\frac{\partial N_{fc}}{\partial t} = \frac{f_p^4 \beta_{\mathrm{TPA}}}{2\hbar\omega_p}|A_p(z,t)|^4 - \frac{N_{fc}(z,t)}{\tau_{fc}}, \tag{8}$$

where τ_{fc} is the free-carrier recombination time. In bulk silicon τ_{fc} is quite large (10 ns or so). In the case of a nanowaveguide, this recombination time is reduced to close to 1 ns because of enhanced surface recombination. However, it remains much larger compared to the pump and signal pulse durations we are dealing with (10 ps or less). For this reason, the second term may be omitted compared to the first one over the pulse duration.

Free carriers generated by TPA change both the real and imaginary part of the effective refractive index associated with the waveguide mode. These changes are governed by the Drude–Lorentz equation which links the complex refractive index to the electron and hole concentrations [32]. The imaginary part leads to free-carrier absorption (FCA) that we consider to be negligeable in this paper. This assumption is reasonable if the repetition rate ν_R of pulses satisfies the condition $\nu_R \tau_{fc} \ll 1$), and the peak intensity remains relatively low ($I_p < 3GW/cm^2$) for pulses of duration around 10 ps [33]. The influence of free carriers on the real part of the complex refractive index leads to FCR. The index change is proportional in this case to the free-carrier density and is equal to $k_c N_{fc}$, where k_c is the FCR coefficient.

2.3 Numerical solution with the split-step Fourier method

In most cases, Eqs. (2), (3) and (8) cannot be solved analytically, and a numerical method must be used to model the propagation and Raman amplification of optical pulses inside a silicon waveguide. We use the well-known split-step Fourier method for this purpose [27]. It makes use of the Fourier representation on an appropriate temporal grid to obtain a set of ordinary differential equations. We split the coupled pump-signal equations into a linear part that is solved in the Fourier domain and a nonlinear part that is solved in the time domain (TPA, Kerr effect and FCR). The Raman term is solved alternatively in the Fourier domain and the time domain because it contains a convolution product. Because these equations are solved alternatively, this method makes the assumption that each part acts independently. However, by choosing a step size along z that is sufficiently small, accurate numerical results can be obtained.

In the following section, we use an approximate analytical method to obtain the effective Raman gain and show that it is reduced from its actual value because of the spectral broadening of pump pulses resulting from SPM and FCR [5]. Numerical simulations provide us data that we compare to our analytical results to show that our simple model is reasonable. Values of various parameters used in our analytical and numerical calculations are specified in Table 1, along with references where these values can be found.

3 Analytical study of Raman amplification of picosecond pulses

3.1 Effective Raman gain

In this section we introduce the concept of an effective Raman gain by focusing only on the Raman term. This requires a solution of Eqs. (6) and (7) with $\alpha_l = 0$. These equations are still difficult to solve. Assuming that $|A_s(z,t)|^2 \ll |A_p(z,t)|^2$ remains valid for all z, we make the undepleted pump approximation and neglect the $R^*(z,t)$ term in the pump equation so that $A_p(z,t) = A_p(0,t)$. The signal equation can be solved in the Fourier domain where it takes the form

$$\frac{\partial \tilde{A}_s}{\partial z} = \frac{i}{(2\pi)^2} f_p^2 f_s^2 g_R \frac{\Gamma_R}{\Omega_R} \tilde{A}_p(z,\omega) \otimes [\tilde{H}_R(\omega - \Omega_{ps})\{\tilde{A}_p^*(z,\omega) \otimes \tilde{A}_s(z,\omega)\}], \tag{9}$$

where $\otimes$ represents the convolution operator defined such that $f \otimes g(x) = \int_{-\infty}^{\infty} f(y)g(x-y)dy$ and we use the convention $\tilde{f}(\omega) = \int_{-\infty}^{\infty} f(t)e^{-i\omega t}dt$ for the Fourier transform.

Next, we assume that both the pump and signal pulses have Gaussian profiles in the time and frequency domains and that these profiles remain Gaussian as the pulses propagate inside the waveguide. We express the optical field $A_j(z,t)$ and its Fourier transform $\tilde{A}_j(z,\omega)$ as follows:

$$A_j(z,t) = A_j(z,0)\exp(-t^2/2T_j^2), \tag{10}$$

$$\tilde{A}_j(z,\omega) = \tilde{A}_j(z,0)\exp(-\omega^2/2\Omega_j^2), \tag{11}$$

where $j = s,\ p$. T_j and Ω_j represent the intensity half-widths at 1/e points related to each other as $\Omega_j = 1/T_j$.

Third, we ignore the effect of the real part of the Raman response responsible for the slow-light effects through Raman dispersion and assume that the imaginary part of $\tilde{H}_R(\Omega)$, related to the Raman gain spectrum known to have a Lorentzian shape, can be approximated with a Gaussian function. We find that the following form approximates the Lorentzian shape reasonably well, close to the gain peak ($\Omega = \Omega_R$) as it corresponds to a fit based on the least-squares method:

$$\mathrm{Im}\left[\tilde{H}_R(\Omega)\right] \approx \frac{\Omega_R}{2\Gamma_R}\exp\left[-\frac{(\Omega-\Omega_R)^2}{2\Gamma_R^2}\right]. \tag{12}$$

Figure 1 compares the Gaussian approximation to the actual Lorentzian shape of the Raman gain spectrum.

With these assumptions and simplifications, we can calculate the Raman term in Eq. (9) in an analytic form. Taking the in-

Parameter Name	Symbol	Value	Reference
Waveguide length	L	1 cm	[5]
Linear losses	α_l	100 m^{-1}	[5]
TPA parameter	β_{TPA}	0.8 cm/GW	[5]
Kerr coefficient	n_2	6×10^{-18} m^2/W	[33]
Raman gain coefficient	g_R	8.9 cm/GW	[5]
Raman linewidth	Γ_R	$\pi \times 105$ GHz	[11]
Raman resonance	Ω_R	$2\pi \times 15.6$ THz	[11]
Carrier lifetime	τ_{fc}	10 ns	[34]
FCR coefficient	k_c	-1.35×10^{-27} m^3	[33]
Signal wavelength	λ_s	1.55 μm	[5]
Pump wavelength	λ_p	1.434 μm	[5]
Local field factor for signal beam	f_s	1.21	[5]
Local field factor for pump beam	f_p	1.21	[5]

TABLE 1 Values of device and material parameters used in calculations

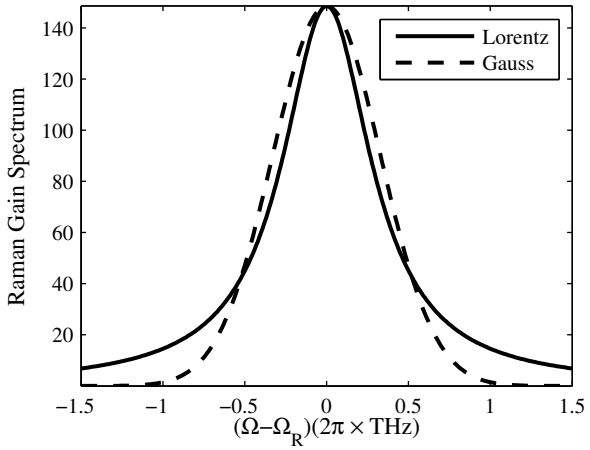

FIG. 1 Comparison of the approximated Gaussian shape to the actual Lorentzian shape of the Raman response spectrum obtained using $\mathrm{Im}[\tilde{H}_R(\Omega)]$

verse Fourier transform, we obtain

$$\frac{\partial A_s}{\partial z} = \frac{1}{2} f_p^2 f_s^2 g_R^{\mathrm{eff}} |A_p(z,0)|^2 A_s(z,0) \exp\left(-\Omega_{\mathrm{eff}}^2 t^2/2\right), \quad (13)$$

where the effective Raman gain g_R^{eff} and the effective amplifier bandwidth Ω_{eff} are defined as

$$\begin{aligned} g_R^{\mathrm{eff}} &= \frac{g_R}{\sqrt{1 + (\Omega_p^2 + \Omega_s^2)/\Gamma_R^2}}, \\ \Omega_{\mathrm{eff}}^2 &= \frac{\Gamma_R^2 (\Omega_s^2 + \Omega_p^2)}{\Gamma_R^2 + (\Omega_s^2 + \Omega_p^2)} + \Omega_p^2. \end{aligned} \quad (14)$$

Ω_{eff} represents the effective bandwidth (B_{eff}) over which the signal pulse can be amplified through SRS in silicon. Table 2 shows that the definition of Ω_{eff} is consistent in several limiting cases with what one would expect intuitively.

To ensure that the formula for g_R^{eff} is applicable in practice in spite of our approximations, we compare it to numerical simulations considering the case in which picosecond signal pulses are amplified using pump pulses with nearly the same spectral bandwidths ($\Omega_p = \Omega_s = \Omega_0$). In the following, we are mainly interested in studying how broadening of the pump spectrum affects the effective Raman gain near the signal-pulse peak. We thus set $t = 0$ in Eq. (13) and assume that the peak pump intensity, $I_p = |A_p(z,0)|^2$, does not change with z. The signal intensity $I_s = |A_s|^2$ then evolves along the amplifier as

$$\frac{dI_s}{dz} = f_p^2 f_s^2 g_R^{\mathrm{eff}} I_p I_s, \qquad g_R^{\mathrm{eff}} = \frac{g_R}{\sqrt{1 + 2\Omega_0^2/\Gamma_R^2}}. \quad (15)$$

Note that $g_R^{\mathrm{eff}} = g_R$ in the CW limit corresponding to $\Omega_0 = 0$ and that it decreases as the SRS regime becomes more transient. Integration of Eq. (15) provides the following solution for the amplification factor:

$$G = \frac{I_s(z)}{I_s(0)} = \exp\left(f_p^2 f_s^2 g_R^{\mathrm{eff}} I_p\right). \quad (16)$$

We plot in Figure 2 the amplification factor G as a function of the input pump intensity for a 1-cm-long silicon waveguide. The symbols represent numerical data that we obtain by solving the full equation (9) using the Raman response function $\tilde{H}_R(\Omega)$ given by equation (5). Different sets correspond to different pump and signal pulse durations. The solid lines are plots of G using the analytical expression with g_R^{eff} given in Eq. (15). The numerical data follows the linear variation in this semi-logarithmic plot at low pump intensities. The slope of each straight line diminishes as the duration of pump pulse decreases, which is consistent with our theoretical prediction and fits well our model. As the intensity increases, the simulations deviate from the analytical model because of the simplifying assumptions that we have made in deriving it (notably that the pulses stay Gaussian and keep their initial bandwidths). However, we are able to account for a decrease in effective Raman gain due to the spectral broadening of the pump. As the pulse duration becomes larger (50 ps), the evolution of G corresponds to the CW regime, as one may expect. Note that the expression of G fits the numerical data better in the extreme cases of very long and very short pulses. This can be understood as follows. In the case of short pulses (transient regime), $\Omega_0 \gg \Gamma_R$ and $\tilde{H}_R(\omega_R)$ can be approximated with a delta function. In the case of long pulses (CW regime), $\Omega_0 \ll \Gamma_R$ and the spectra of both the pump and signal pulses are much narrower (close to a delta function) than the Raman

Pump Regime	Signal Regime	B_{eff}	g_R^{eff}	SRS Regime
$\Omega_p = 0$	$\Omega_s = 0$	$\Omega_{\text{eff}} = 0$	g_R	CW pump and signal
$\Omega_p = 0$	$\Omega_s \gg \Gamma_R$	$\Omega_{\text{eff}} = \Gamma_R$	0	Transient Signal, CW pump
$\Omega_p = 0$	$\Omega_s \ll \Gamma_R$	$\Omega_{\text{eff}} = \Omega_s$	g_R	signal Pulse, CW pump
$\Omega_p \gg \Gamma_R$	$\Omega_s = 0$	$\Omega_{\text{eff}} = \Omega_p$	0	Transient Pump, CW signal
$\Omega_p \ll \Gamma_R$	$\Omega_s = 0$	$\Omega_{\text{eff}} = \Omega_p$	g_R	Pulsed pump, CW signal

TABLE 2 Limiting cases for the effective gain amplifier bandwidth

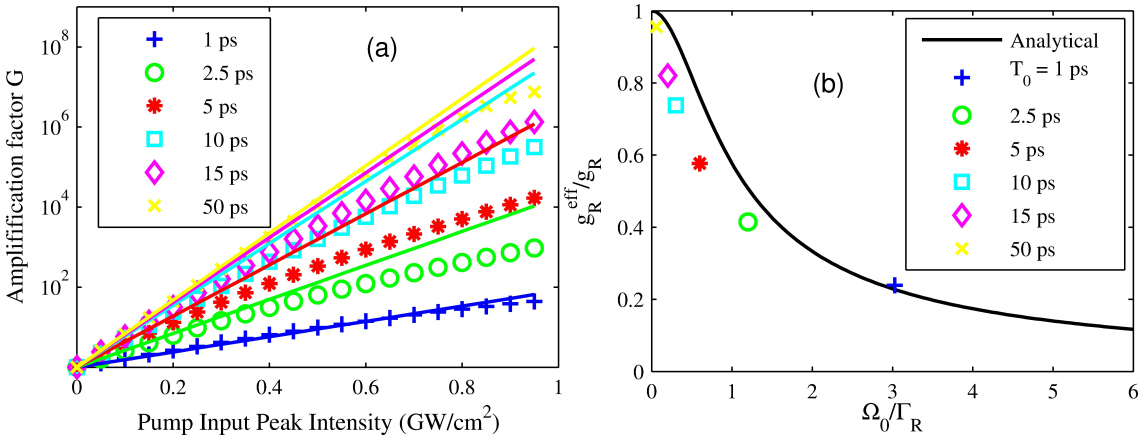

FIG. 2 (a) Amplification factor as a function of peak intensity $I_p(0)$ for several pump pulse durations. Symbols show the numerical data obtained by solving Eq. (9). Solid lines correspond to the analytical formula (16). (b) Reduction in the Raman gain, g_R^{eff}/g_R, as a function of Ω_0/Γ_R calculated using Eq. (15) with $g_R = 8.9$ cm/GW. Symbols are obtained using numerical data in part (a).

gain spectrum. In those regimes, the exact shape of the Raman spectrum (gaussian or lorentzian) is non-critical and has little influence.

3.2 Influence of TPA on SRS

In this subsection we study how TPA further reduces the amplification factor in a silicon Raman amplifier. For this purpose, we neglect the free-carrier terms in Eqs. (2) and (3), include SRS in terms of g_R^{eff} given in Eq. (15), and neglect pump depletion due to SRS. Using $I_m = |A_m|^2$ $(m = p, s)$, the pump and signal intensities are then found to satisfy

$$\frac{\partial I_s}{\partial z} = f_p^2 f_s^2 (g_R^{\text{eff}} - \beta_{\text{XPA}}) I_p I_s - \alpha_l I_s, \tag{17}$$

$$\frac{\partial I_p}{\partial z} = -f_p^4 \beta_{\text{TPA}} I_p^2 - \alpha_l I_p. \tag{18}$$

The pump equation (18) can be solved easily in terms of the input pump intensity $I_p(0,t)$ to obtain

$$I_p(z,t) = \frac{I_p(0,t) e^{-\alpha_l z}}{1 + \alpha_{\text{TPA}} L_{\text{eff}}(z)}, \tag{19}$$

where $L_{\text{eff}}(z) = (1 - e^{-\alpha_l z})/\alpha_l$ is the effective length and we have introduced an effective TPA-loss parameter as

$$\alpha_{\text{TPA}} = f_p^4 \beta_{\text{TPA}} I_p(0,0). \tag{20}$$

In practice, this last term is not constant and depends on the time profile of $I_p(0,t)$, but we replace it with its maximum value at the pulse center, which is needed because we make the assumption that the shape of the pump remains Gaussian. This replacement is valid for low TPA regimes and overestimates its influences for higher TPA regimes.

Knowing the evolution of the pump intensity along the waveguide length, we use Eq. (19) in Eq. (17) and solve it analytically. The solution is used to obtain the on-off gain $G_{\text{on-off}}$ defined as the ratio of output signal power with the pump on and off. On the decibel scale, this gain is given by

$$\begin{aligned} G_{\text{on-off}}^{\text{dB}} &= 10 \log_{10} \left[\frac{I_s(L)}{I_s(0) e^{-\alpha_l L}} \right] \\ &= \frac{f_s^2}{f_p^2} \frac{(g_R^{\text{eff}} - \beta_{\text{XPA}})}{\beta_{\text{TPA}}} \left(1 + \alpha_{\text{TPA}} L_{\text{eff}}\right)_{\text{dB}}. \end{aligned} \tag{21}$$

The solid lines in Figure 3 show the on-off gain as a function of $(1 + \alpha_{\text{TPA}} L_{\text{eff}})_{\text{dB}}$ for several pulse durations in the range of 1–50 ps. The numerical results are shown again as symbols. Compared to the results in Figure 2, we observe that the slopes of the solid lines are reduced because of the TPA process. We also note that the analytical curves provide a satisfactory fit of the numerical data for low values of $(1 + \alpha_{\text{TPA}} L_{\text{eff}})_{\text{dB}}$. We point out that the expression of $G_{\text{on-off}}$ depends on the local field factors f_s and f_p as a ratio. Although α_{TPA} contains a factor f_p^4, its influence on the on-off gain is logarithmic. One way to enhance the amplification process consists of localizing the signal wave much more than the pump wave to maximize the ratio f_s^2/f_p^2. It is interesting to note, that in the absence of TPA [see Eq. (16)], localizing both the pump and the signal is advantageous to Raman amplification.

4 Spectral broadening of the pump pulse and its influence on SRS

In the preceding section we obtained an analytical solution describing how the peak intensities of the signal and pump

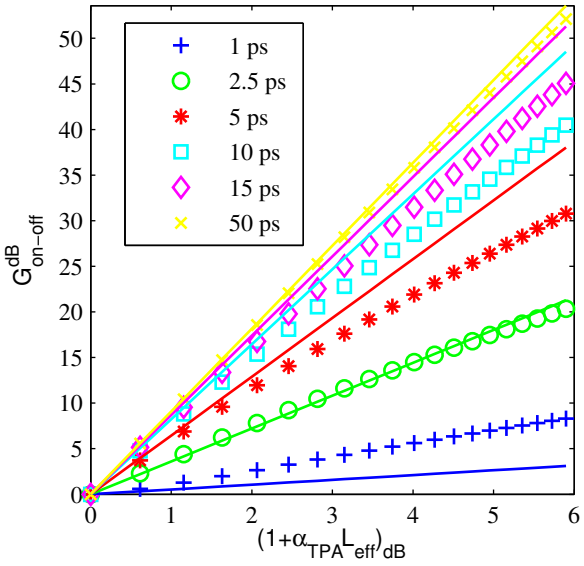

FIG. 3 On-Off gain G_{on-off}, plotted as a function of $(1+\alpha_{TPA}L_{eff})_{dB}$ for different pulse durations. Markers represent the numerical data obtained by solving equations (17) and (18), taking into account TPA, XPA, linear absorption and SRS. Solid lines correspond to the analytical formula.

pulses evolve as they propagate through a Raman amplifier while experiencing Raman gain through SRS and losses through TPA (and other linear mechanisms). The next step is to consider how the SPM and FCR phenomena affect the phase of the pump pulse and modify the amplification process. Spectral broadening of the pump pulse induced by SPM and FCR is expected to decrease further the effective Raman gain once the pump's spectral bandwidth becomes comparable to or exceeds the bandwidth of the Raman gain spectrum.

4.1 Nonlinear phase equation

Using $A_p = \sqrt{I_p}\exp(i\phi_p)$ in the pump equation (3), we can obtain two equations, one giving the evolution of intensity I_p (solved in Section 3), and the other giving the evolution of the pump phase ϕ_p. This phase equation is given by

$$\frac{\partial \phi_p}{\partial z} = k_p f_p^2 \left[f_p^2 n_2 I_p(z,t) + k_c N_{fc}(z,t) \right], \qquad (22)$$

where $I_p(z,t)$ is given in Eq. (19) and $N_{fc}(z,t)$ is obtained by integrating Eq. (8). If we neglect the recombination time assuming pump pulses shorter than 10 ps, $N_{fc}(z,t)$ is given by

$$N_{fc}(z,t) = \frac{f_p^4 \beta_{TPA}}{2\hbar\omega_p} I_p^2(z,0) \sqrt{\frac{\pi}{2}} \frac{T_0}{2} \left[1 + \mathrm{erf}\left(\frac{\sqrt{2}t}{T_0} \right) \right]. \qquad (23)$$

Using this, Eq. (22) can be integrated with respect to z and provides the total accumulated phase during propagation over the amplifier length L in the form

$$\phi_p(L,t) = (\rho_1 + \rho_2)\phi_{fc}(t) - \rho_2(\alpha_{TPA}/\alpha_l)\phi_K(t), \qquad (24)$$

where the Kerr and FCR contributions have been separated using the definitions

$$\phi_K(t) = k_p f_p^4 n_2 I_p(0,t) L_{eff}, \qquad (25)$$

$$\phi_{fc}(t) = k_p f_p^2 k_c N_{fc}(0,t) L_{eff}, \qquad (26)$$

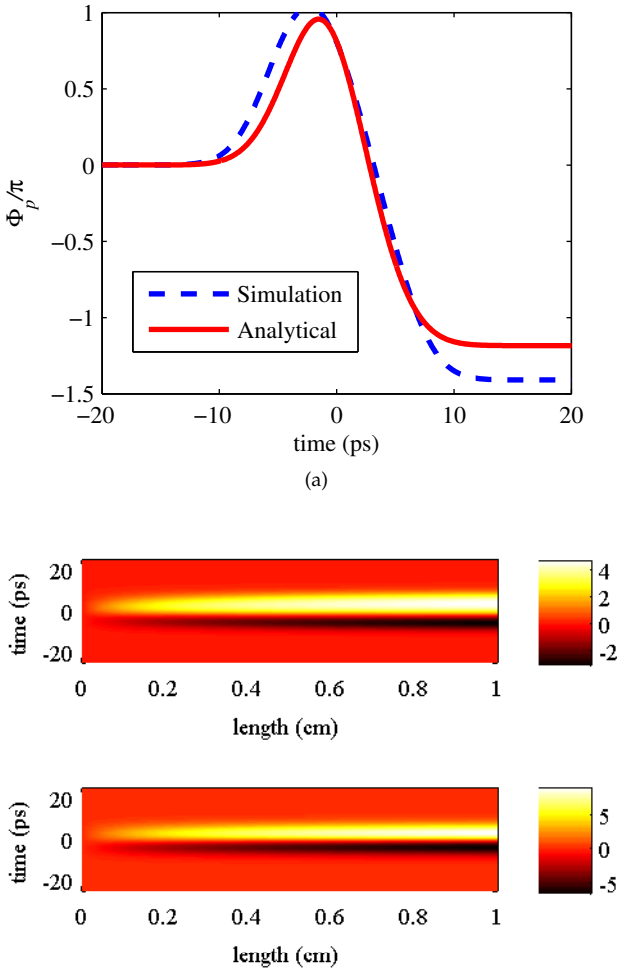

FIG. 4 (a) Nonlinear phase of the pump pulse plotted as a function of time at the ouput of a 1-cm long waveguide. The two curves compare the analytical solution with the numerical data obtained using Eqs. (3) (without considering pump depletion through SRS) with 5-ps pump pulses with a peak intensity of 3 GW/cm^2. (b) Normalized frequency chirp, $\Delta\omega(t)/\Omega_0$, plotted as a function of distance. The top and bottom plots show the numerical and analytical results, respectively.

and we have introduced two new parameters as

$$\rho_1 = \frac{1+\alpha_l/\alpha_{TPA}}{1+\alpha_{TPA}L_{eff}}, \qquad (27)$$

$$\rho_2 = \frac{\alpha_l}{\alpha_{TPA}^2 L_{eff}} \left[\alpha_l L + \ln\left(\frac{1-\alpha_l L_{eff}}{1+\alpha_{TPA}L_{eff}} \right) \right]. \qquad (28)$$

Figure 4a compares the analytically calculated phase to the numerically simulated phase using the same device parameters. The agreement is relatively good in spite of several simplifying approximations we have made. The Kerr part, $\phi_K(t)$, follows the intensity profile of the pump pulse. However, free carriers produce a phase shift $\phi_{fc}(t)$ that builds up as an error function. Furthermore, given that the signs of the nonlinear Kerr index n_2 and the FCR coefficient k_c are opposite, the nonlinear phase increases over the leading part of the pulse during which free carriers are created but soon after it begins to decrease and becomes negative near the trailing edge of the pulse.

From Eq. (24), we can calculate the frequency chirp or the in-

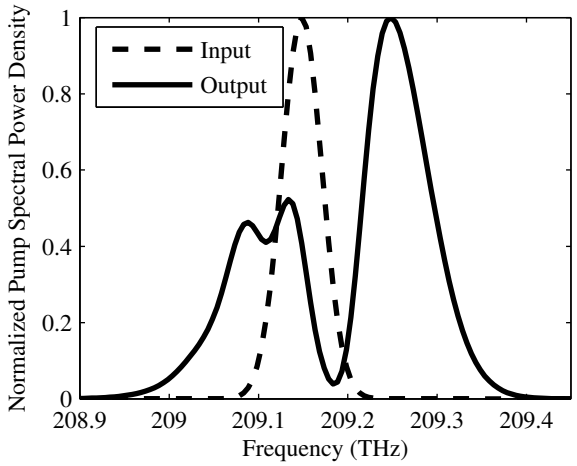

FIG. 5 Numerically simulated output pump spectrum for a 1-cm-long silicon waveguide when input pump intensity is 3 GW/cm^2.

stantaneous frequency shift $\Delta\omega(t)$ by differentiating $\phi_p(L,t)$ with respect to time. Figure 4b shows how this chirp builds up along the amplifier length using a surface plot in which different colors show different values of $\Delta\omega(t)/\Omega_0$. This figure shows the classical behavior that the leading edge of the pulse is red-shifted whereas its trailing edge is blue-shifted. The frequency chirp due to the Kerr effect, as governed by pulse intensity derivative, is negative on the leading edge of the pulse and positive on the trailing edge, whereas the FCR chirp governed directly by the pulse intensity is always positive. As a result, they have the opposite signs near the leading edge but have the same sign near the trailing edge. This means that a greater part of the pulse exhibits a blue-shift. Such a chirp behavior is consistent with the numerically simulated spectrum of the pulse shown in Figure 5 where the blue-shifted peak has larger amplitude than the red-shifted one.

4.2 Characterization of the spectral broadening

In this subsection we estimate the spectral broadening of the pump pulse using the concept of the root-mean-square (rms) bandwidth and study how this width changes with the pump pulse energy. To do so, we use a method first used in 1985 for studying SPM-induced spectral broadening in optical fibers [35] and extend it by including the FCR contribution as well. The rms spectral width $\Delta\omega_\sigma$ is found by computing the variance as

$$(\Delta\omega_\sigma)^2 = \left\langle \omega^2 \right\rangle - \langle\omega\rangle^2 = \frac{\int \omega^2 |\tilde{A}_p(\omega)|^2 d\omega}{\int |\tilde{A}_p(\omega)|^2 d\omega} - \left[\frac{\int \omega |\tilde{A}_p(\omega)|^2 d\omega}{\int |\tilde{A}_p(\omega)|^2 d\omega}\right]^2. \quad (29)$$

Although $\tilde{A}_p(\omega)$ cannot be calculated in closed form, we know the complex amplitude of the pump pulse in the time domain:

$$A_p(t) = \sqrt{I_p(L,0)}\exp\left[-\frac{t^2}{2T_0^2} + i\phi_p(L,t)\right]. \quad (30)$$

We thus use the following moment formula relating the n^{th}-order moment in the Fourier domain to the n^{th} derivative in the time domain [35]:

$$\int \omega^n \tilde{f}(\omega) d\omega = 2\pi(-i)^n f^{(n)}(0). \quad (31)$$

Using Eq. (31) and the Wiener-Khintchin theorem, we can express $\Delta\omega_\sigma$ in terms of $A_p(t)$ as

$$(\Delta\omega_\sigma)^2 = \frac{\int |A_p'(\tau)|^2 d\tau}{\int |A_p(\tau)|^2 d\tau} + \left[\frac{\int A_p^*(\tau) A_p'(\tau) d\tau}{\int |A_p(\tau)|^2 d\tau}\right]^2, \quad (32)$$

where a prime denotes the first derivative of the function. All integrals can be calculated in a closed form using Eqs. (24), (30), and (32). The final result is given by

$$(\Delta\omega_\sigma)^2 = \Omega_0^2\left[\frac{1}{2} + \frac{8}{\pi}\left(\frac{1}{\sqrt{5}} - \frac{1}{3}\right)(\rho_1+\rho_2)^2\phi_{fc}^2(0) + \frac{2}{3\sqrt{3}}\rho_3^2\phi_K^2(0)\right], \quad (33)$$

where $\rho_3 = (\alpha_{\mathrm{TPA}}/\alpha_l)\rho_2$.

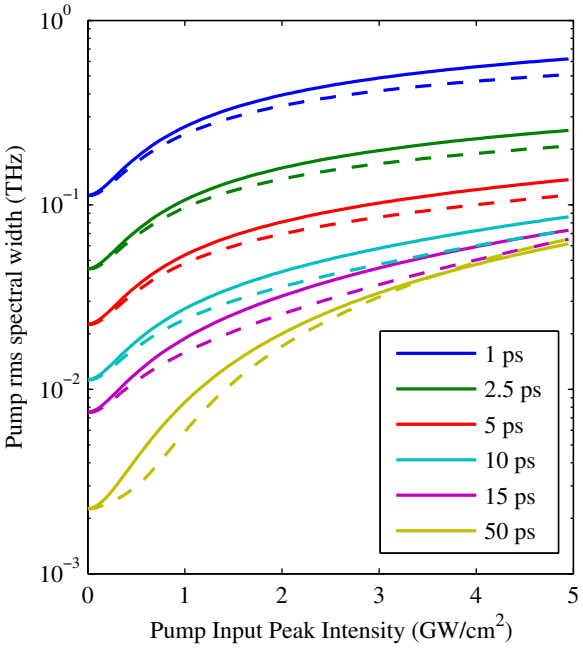

FIG. 6 The rms spectral width $\Delta\omega_\sigma$ plotted as a function of peak intensity of input pump pulses of different pulse durations. The dashed curves show the output spectrum widths obtained numerically using Eqs. (3) (without considering pump depletion through SRS) whereas solid lines correspond to Eq. (33).

Solid lines in Figure 6 show $\Delta\omega_\sigma$ as a function of the peak intensity of the input pump pulse using the analytical result in Eq. (33). The dashed lines show the results obtained numerically for different pulse durations in the range of 1–50 ps. We can see that the agreement between the two methods is reasonable and improves for longer pulse durations. Differences between the two curves, especially for shorter pulse durations results from the considerable deformation undergone by the larger spectra for large values of the pump intensity as is evident in Figure 5.

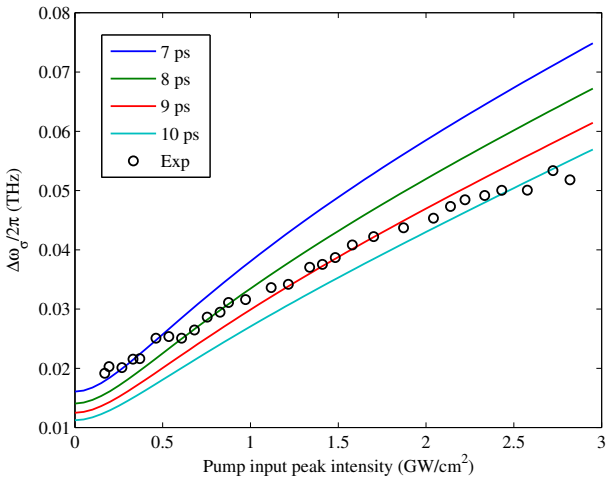

FIG. 7 Comparison between the rms spectral width of the pump-spectra measured in [5] (open circles) and the theoretical values given by Eq. (33) for pulse durations between 7 and 10 ps (solid lines).

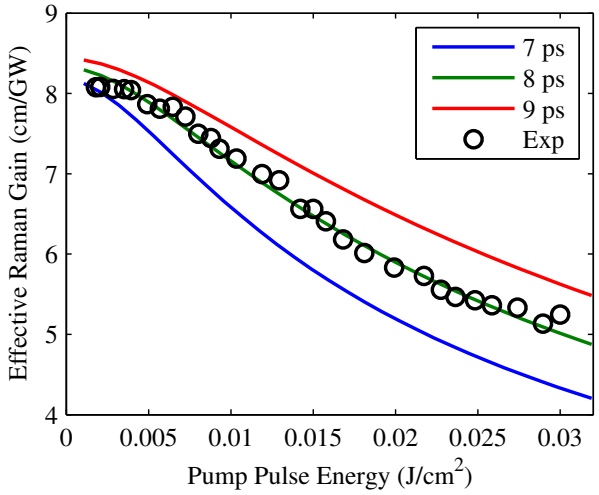

FIG. 8 Effective Raman gain g_R^{eff} plotted for several pulse durations as a function of pump pulse energy at the input of the waveguide. The solid lines show the analytical result using Eq. (15) and the circles correspond to the experimental data in Ref. [5].

5 Influence of pump-spectrum broadening on effective Raman gain

In this section we compare the predictions of our approximate analytical model with the recent experimental results of Kroeger *et al.* [5] showing the saturation of the Raman gain with increasing pump pulse energies. Besides the observed pump-spectrum broadening and saturation of the Raman amplification, the measurements and data analysis method are reported in [5] and enabled the determination of the injected pump intensities. A comparison between our theoretical model and these experimental data is made in this section.

5.1 Spectral width of the SPM-broadened pump pulses

From the output pump-spectra measured for injected pump intensities varying from 0.2 up to 2.6 GW/cm^2 [5], we calculated the experimental rms spectral width $\Delta\omega_\sigma$ using the expression of Eq. (29). They are plotted in figure 7 with open circles as a function of the peak intensity. On the same graph, we plot with solid lines the theoretical values given by Eq. (33) for pulse durations varying from 7 to 10 ps corresponding to the range of the experimental pulse duration. Indeed, from the measured pump spectrum and assuming that the input pump pulses are unchirped, we estimate an experimental value of $T_0 = 7$ ps for the pump pulse (corresponding to the 15 ps full width of the pulse considered in Ref. [5]). The comparison shows that our analytical expression for the rms spectral width is in good agreement with the experimental observations considering that the numerical simulations that are slightly below the analytical curves (Fig. 6), should correspond better to the experimental data for a given pulse duration.

5.2 Reduction of the effective Raman gain

From Eq. (33), we obtain the effective $1/e$ half-bandwidth for the SPM-broadened pump spectrum using $\Omega = \sqrt{2}\Delta\omega_\sigma$ and use this value in Eq. (14) to obtain the effective Raman gain g_R^{eff} as a function of pump pulse energy. Noting that the effects of XPM are relatively small for the signal pulse, whose bandwidth is mostly set by the Raman gain spectrum that does not undergo any broadening, we make the approximation that $\Omega_s \approx 0$ in Eq. (14), because g_R^{eff} is mostly influenced by the broadening of the pump bandwidth. The results are shown by solid lines in Figure 8 for several values of the pump pulse duration T_0. The measured experimental data of Ref. [5], taken for pump pulses with $T_0 = 7$ ps, are shown by circles in this figure. In both cases, the effective Raman gain decreases as the pump energy increases. According to our theoretical model, this decrease is due to SPM-induced spectral broadening of the pump pulses. Physically speaking, when the broadening becomes large enough that the pump bandwidth begins to exceed the Raman gain bandwidth Γ_R, only a portion of pump energy can be used for SRS. The convolution present in Eq. (9) takes into account this feature mathematically and it produces a reduced effective gain. We also see, as was pointed out in section 3, that the gain is further reduced for shorter pump pulses. We note from Figure 8 that the best agreement with the experimental data is obtained for a theoretical pulse duration of $T_0 = 8$ ps, in agreement with our estimation of the experimental pulse duration of 7 ps.

The important point to note is that our analytical model can predict the experimental behavior remarkably well in spite of several simplifying approximations made during our analysis.

5.3 Influence of the light-localization effect

Besides the prediction of the reduction of the effective Raman gain, our analytical model can predict the performance of a Raman amplifier based on a slow-mode waveguide for which, both the pump and Stokes signals are localized. We have already seen that, even if light localization of both pump and Stokes signals is favorable in a pure Raman media, this point must be revised in presence of two-photon absorption. Con-

sidering Eq. (21), it seems that in presence of TPA, it is advantageous to localize the Stokes signal more than the pump. This tendency will be reinforced if spectral broadening is taken into account. To show this, we have calculated the On-Off Gain in different localization situations and plotted in figure 9 the values as a function of $(1+\alpha_{\mathrm{TPA}}L_{\mathrm{eff}})_{\mathrm{dB}}$. We chose two values for the local field factor: 1.21 corresponding to our waveguide and 1.5 corresponding to a W1 photonic crystal waveguide with a reduced group velocity around $c/8$ [30].

We first consider a situation of an identical localization effect for pump and signal in order to avoid any temporal walk-off between pulses. When $f_p = f_s = 1.5$ a maximum gain of 23 dB, similar to the maximum gain obtained with $f_p = f_s = 1.21$, is reached for a lower input pump intensity. Beyond this value, i.e. for $(1+\alpha_{\mathrm{TPA}}L_{\mathrm{eff}}) > 5\,\mathrm{dB}$, a stronger saturation of the on-off Raman gain occurs for $f_p = f_s = 1.5$ because the spectral broadening is more enhanced than in the case $f_p = f_s = 1.21$.

In a situation where $f_p \neq f_s$, one has to mention the inevitable reduction of the on-off Raman gain through the temporal walk-off effect, which is not described by our model. In the following discussion, considering one pulse duration and two local field factors, one has to consider a maximum effective length L_{eff} that minimizes the temporal walk-off between pump and signal pulses. By doing so, we wish to emphasize on the effect of the spectral broadening on the gain amplification. We can see that the two situations $f_p = 1.21$, $f_s = 1.5$ (green curve in Fig. 9) and $f_p = 1.5$, $f_s = 1.21$ (magenta curve in Fig. 9) nominally identical in a pure Raman media (or at low pump power when two photon absorption is negligible) very rapidly diverge when the pump power increases with a difference in the maximum accessible gain of 20 dB. It is clear from these curves that when the pump is more localized ($f_p > f_s$), the spectral broadening will be enhanced and saturation of the gain will appear sooner (for $(1+\alpha_{\mathrm{TPA}}L_{\mathrm{eff}}) \approx 3\,\mathrm{dB}$), because more free-carriers are generated (contrary to the case when $f_s > f_p$). This prevents high amplification gain.

Even though it is non-exhaustive, this first result clearly shows that light localization completely reorganizes the hierarchy between the different nonlinearities and that careful analysis is necessary to optimize a device in the slow-mode regime. Analytical models, such as the one developed here, are essential tools to make such a study as they give easy access to the influence of the different parameters on the quantities that need to be optimized.

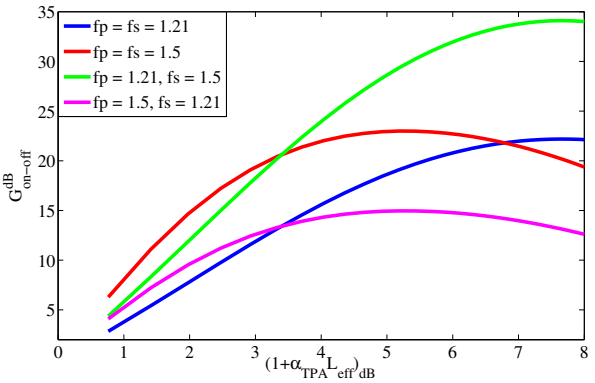

FIG. 9 Calculated on-off Raman gain $G_{\mathrm{on-off}}$ given by Eq. (21) as a function of $(1+\alpha_{\mathrm{TPA}}L_{\mathrm{eff}})_{\mathrm{dB}}$ for different localization situations and taking into account the theoretical SPM-broadening of the pump pulse. The local field factors for pump and signal are set equal to 1.21 or 1.5, corresponding to a group velocity equal to $c/5$ and $c/8$, respectively.

6 Conclusions

In this paper we have solved the Raman amplification problem for silicon waveguides in the regime in which both the pump and signal pulses are relatively short (~10 ps) but still wide enough that their duration exceeds the phonon lifetime (about 3 ps). We used a well-known model based on the coupled pump-signal amplitude equations for numerical simulations because such a model includes all competing nonlinear effects such as the Kerr effect, TPA, FCA, and FCR that take place simultaneously. However, numerical simulations do not provide much physical insight. For this reason, we also developed an approximate analytic approach for solving the Raman amplification problem. We introduced the concept of an effective Raman gain coefficient and showed analytically how this effective Raman gain depends on the pump bandwidth. Since the pump spectrum broadens inside the silicon waveguide owing to a combination of the Kerr effect and FCR, these two phenomena affect the Raman amplification process considerably. We were able to obtain an analytical form of the nonlinear phase accumulated during propagation inside a silicon waveguide, which enabled us to calculate the total spectral broadening experienced by a pump pulse as it propagates through a silicon nanowaveguide in the nonlinear regime. Using this result, we were able to predict changes in the effective Raman gain as a function of the pump pulse energy and compare the results to the recent experimental data. This comparison shows that our model is reasonable and captures all essential physics.

It should be noted that our analysis includes the local-field factors that take into account the enhancement of the pump and signal fields in silicon nanowaveguides. This enhancement can be controlled by reducing the group index (for example in slow-light devices) or by strong confinement (e.g., using microcavities). This feature widens the scope of our analysis because it provides insight into the study of slow-mode or high-localization Raman devices. For instance, strong localization of the pump and signal beams will prove to be detrimental to Raman amplification because of a simultaneous enhancement of the spectral broadening of pump pulses. This point is of crucial importance for designing silicon-based Raman amplifiers and lasers.

We should stress one more important point. Although we have focused on a specific Raman amplification problem in silicon waveguides, our analytical approach is quite general and can be used to study the transient Raman amplification of pulses in a variety of media, including molecular gases, optical fibers, and other semiconductor materials. The main conclusion of our paper is that spectral broadening of pump pulses reduces the extent of Raman-induced transfer of pump

pulse energy to signal pulses in all Raman-active media in which the Kerr effect occurs simultaneously with SRS.

Acknowledgments

The authors in France acknowledge the 'Triangle de la Physique' (RTRA) and the 'Ecole Doctorale Ondes et Matiere' (EDOM) for financial support. The work of G. P. Agrawal in USA was supported by the National Science Foundation Award ECCS-0801772.

References

[1] M. Dinu, F. Quochi, and H. Garcia, "Third-order nonlinearities in silicon at telecom wavelengths", Appl. Phys. Lett. **82**, 2954–2956 (2003).

[2] R. Dekker, N. Usechak, M. Forst, and A. Driessen, "Ultrafast nonlinear all-optical processes in silicon-on-insulator waveguides", J. Phys. D Appl. Phys. **40**, R249–R271 (2007).

[3] D. Miller, "Optical interconnects to silicon", IEEE J. Sel. Top. Quant. **6**, 1312 –1317 (2000).

[4] T. Barwicz, H. Byun, F. Gan, C. W. Holzwarth, M. A. Popovic, P. T. Rakich, M. R. Watts, E. P. Ippen, F. X. Kärtner, H. I. Smith, J. S. Orcutt, R. J. Ram, V. Stojanovic, O. O. Olubuyide, J. L. Hoyt, S. Spector, M. Geis, M. Grein, T. Lyszczarz, and J. U. Yoon, "Silicon photonics for compact, energy-efficient interconnects", J. Opt. Netw. **6**, 63–73 (2007).

[5] F. Kroeger, A. Ryasnyanskiy, A. Baron, N. Dubreuil, P. Delaye, R. Frey, G. Roosen, and D. Peyrade, "Saturation of the Raman amplification by self-phase modulation in silicon nanowaveguides", Appl. Phys. Lett. **96**, 241102 (2010).

[6] R. Claps, V. Raghunathan, D. Dimitropoulos, and B. Jalali, "Influence of nonlinear absorption on raman amplification in silicon waveguides", Opt. Express **12**, 2774–2780 (2004).

[7] T. K. Liang and H. K. Tsang, "Efficient raman amplification in silicon-on-insulator waveguides", Appl. Phys. Lett. **85**, 3343–3345 (2004).

[8] R. Espinola, J. Dadap, J. Richard Osgood, S. McNab, and Y. Vlasov, "Raman amplification in ultrasmall silicon-on-insulator wire waveguides", Opt. Express **12**, 3713–3718 (2004).

[9] T. Liang, L. Nunes, M. Tsuchiya, K. Abedin, T. Miyazaki, D. V. Thourhout, W. Bogaerts, P. Dumon, R. Baets, and H. Tsang, "High speed logic gate using two-photon absorption in silicon waveguides", Opt. Commun. **265**, 171 – 174 (2006).

[10] D. Moss, L. Fu, I. Littler, and B. Eggleton, "Ultrafast all-optical modulation via two-photon absorption in silicon-on-insulator waveguides", Electron. Lett. **41**, 320 – 321 (2005).

[11] Q. Lin, O. J. Painter, and G. P. Agrawal, "Nonlinear optical phenomena in silicon waveguides: modeling and applications", Opt. Express **15**, 16604–16644 (2007).

[12] H. K. Tsang, C. S. Wong, T. K. Liang, I. E. Day, S. W. Roberts, A. Harpin, J. Drake, and M. Asghari, "Optical dispersion, two-photon absorption and self-phase modulation in silicon waveguides at 1.5 μm wavelength", Appl. Phys. Lett. **80**, 416–418 (2002).

[13] O. Boyraz, T. Indukuri, and B. Jalali, "Self-phase-modulation induced spectral broadening in silicon waveguides", Opt. Express **12**, 829–834 (2004).

[14] E. Dulkeith, Y. A. Vlasov, X. Chen, N. C. Panoiu, and J. Richard M. Osgood, "Self-phase-modulation in submicron silicon-on-insulator photonic wires", Opt. Express **14**, 5524–5534 (2006).

[15] T.-K. Liang and H.-K. Tsang, "Nonlinear absorption and raman scattering in silicon-on-insulator optical waveguides", IEEE J. Sel. Top. Quant. **10**, 1149 – 1153 (2004).

[16] D. Moss, L. Fu, I. Littler, and B. Eggleton, "Ultrafast all-optical modulation via two-photon absorption in silicon-on-insulator waveguides", Electron. Lett. **41**, 320–321 (2005).

[17] R. Claps, D. Dimitropoulos, Y. Han, and B. Jalali, "Observation of raman emission in silicon waveguides at 1.54 μm", Opt. Express **10**, 1305–1313 (2002).

[18] M. A. Foster, A. C. Turner, J. E. Sharping, B. S. Schmidt, M. Lipson, and A. L. Gaeta, "Broad-band optical parametric gain on a silicon photonic chip", Nature **441**, 960–963 (2006).

[19] H. Fukuda, K. Yamada, T. Shoji, M. Takahashi, T. Tsuchizawa, T. Watanabe, J. ichi Takahashi, and S. ichi Itabashi, "Four-wave mixing in silicon wire waveguides", Opt. Express **13**, 4629–4637 (2005).

[20] H. Rong, A. Liu, R. Nicolaescu, M. Paniccia, O. Cohen, and D. Hak, "Raman gain and nonlinear optical absorption measurements in a low-loss silicon waveguide", Appl. Phys. Lett. **85**, 2196–2198 (2004).

[21] Q. Xu, V. R. Almeida, and M. Lipson, "Demonstration of high raman gain in a submicrometer-size silicon-on-insulator waveguide", Opt. Lett. **30**, 35–37 (2005).

[22] H. Rong, R. Jones, A. Liu, O. Cohen, D. Hak, A. Fang, and M. Paniccia, "A continuous-wave raman silicon laser", Nature **433**, 725–728 (2005).

[23] O. Boyraz and B. Jalali, "Demonstration of a silicon Raman laser", Opt. Express **12**, 5269–5273 (2004).

[24] Q. Xu, V. Almeida, and M. Lipson, "Time-resolved study of Raman gain in highly confined silicon-on-insulator waveguides", Opt. Express **12**, 4437–4442 (2004).

[25] A. Liu, H. Rong, M. Paniccia, O. Cohen, and D. Hak, "Net optical gain in a low loss silicon-on-insulator waveguide by stimulated Raman scattering", Opt. Express **12**, 4261–4268 (2004).

[26] D. R. Solli, P. Koonath, and B. Jalali, "Broadband Raman amplification in silicon", Appl. Phys. Lett. **93**, 191105 (2008).

[27] G. P. Agrawal, *Nonlinear Fiber Optics* (Academic Press, 2007), 4th ed.

[28] L. Razzari, D. Trager, M. Astic, P. Delaye, R. Frey, G. Roosen, and R. Andre, "Kerr and four-wave mixing spectroscopy at the band edge of one-dimensional photonic crystals", Appl. Phys. Lett. **86**, 231106 (2005).

[29] P. Delaye, M. Astic, R. Frey, and G. Roosen, "Transfer-matrix modeling of four-wave mixing at the band edge of a one-dimensional photonic crystal", J. Opt. Soc. Am. B **22**, 2494–2504 (2005).

[30] A. Baron, A. Ryasnyanskiy, N. Dubreuil, P. Delaye, Q. V. Tran, S. Combrié, A. de Rossi, R. Frey, and G. Roosen, "Light localization induced enhancement of third order nonlinearities in a GaAs photonic crystal waveguide", Opt. Express **17**, 552–557 (2009).

[31] C. Monat, B. Corcoran, D. Pudo, M. Ebnali-Heidari, C. Grillet, M. Pelusi, D. Moss, B. Eggleton, T. White, L. O'Faolain, and T. Krauss, "Slow light enhanced nonlinear optics in silicon photonic crystal waveguides", IEEE J. Sel. Top. Quant. **16**, 344 –356 (2010).

[32] A. A. Said, M. Sheik-Bahae, D. J. Hagan, T. H. Wei, J. Wang, J. Young, and E. W. V. Stryland, "Determination of bound-electronic and

free-carrier nonlinearities in ZnSe, GaAs, CdTe, and ZnTe", J. Opt. Soc. Am. B **9**, 405–414 (1992).

[33] L. Yin and G. P. Agrawal, "Impact of two-photon absorption on self-phase modulation in silicon waveguides", Opt. Lett. **32**, 2031–2033 (2007).

[34] S. Roy, S. K. Bhadra, and G. P. Agrawal, "Raman amplification of optical pulses in silicon waveguides: effects of finite gain bandwidth, pulse width, and chirp", J. Opt. Soc. Am. B **26**, 17–25 (2009).

[35] S. C. Pinault and M. J. Potasek, "Frequency broadening by self-phase modulation in optical fibers", J. Opt. Soc. Am. B **2**, 1318–1319 (1985).